PHYSICAL REVIEW A **94**, 011401(R) (2016)

Driven-dissipative many-body systems with mixed power-law interactions: Bistabilities and temperature-driven nonequilibrium phase transitions

N. Šibalić,[1,*] C. G. Wade,[1] C. S. Adams,[1] K. J. Weatherill,[1] and T. Pohl[2]

[1]*Joint Quantum Center (JQC) Durham-Newcastle, Department of Physics, Durham University, South Road, Durham, DH1 3LE, United Kingdom*

[2]*Max Planck Institute for the Physics of Complex Systems, D-01187 Dresden, Germany*

(Received 7 December 2015; published 14 July 2016)

We investigate the nonequilibrium dynamics of a driven-dissipative spin ensemble with competing power-law interactions. We demonstrate that dynamical phase transitions as well as bistabilities can emerge for asymptotic van der Waals interactions, but critically rely on the presence of a slower decaying potential core. Upon introducing random particle motion, we show that a finite gas temperature can drive a phase transition with regards to the spin degree of freedom and eventually leads to mean-field behavior in the high-temperature limit. Our work reconciles contrasting observations of recent experiments with Rydberg atoms in the cold-gas and hot-vapor domain, and introduces an efficient theoretical framework in the latter regime.

DOI: 10.1103/PhysRevA.94.011401

The idea that matter rapidly relaxes towards a thermal ensemble [1] has led to a profound understanding of many macroscopic phenomena within the powerful framework of equilibrium statistical physics. More recently, the experimental success in realizing synthetic many-body systems with controllable dissipation has motivated broad explorations of nonthermal steady states [2]. Examples include cold atoms in cavities [3], semiconductor exciton-polariton condensates [4], trapped ion crystals [5], and laser-driven Rydberg gases [6]. The interplay of coherent and dissipative dynamics in such driven-dissipative systems generates nonequilibrium phases and transitions that may have no equilibrium equivalent. An evident example of such distinct behavior is the emergence of multiple steady states.

Signatures of bistable many-body phases and hysteretic behavior are reported in experiments on cold [7] and thermal [8] Rydberg gases, which offer controllable particle interactions, dissipation, and coherent driving. While the basic physics suggests a conceptually simple description in terms of a dissipative spin ensemble [9–21], understanding its many-body dynamics has proved challenging. Lattice mean field (MF) descriptions [12,14], for instance, relate cold atom experiments [7] to the formation of a bistable steady state, while variational calculations [17,18] suggest an interpretation in terms of a first-order phase transition. On the other hand, MF predictions agree with observations in thermal vapor experiments [8,14], but are in conflict with field-theoretical [19] and exact numerical results of one-dimensional spin chains [13]. In two dimensions, MF and variational approaches predict the emergence of antiferromagnetic phases at strong dissipation [9,12,18], contradicting corresponding numerical simulations [20].

Here we address this problem through numerical studies of the driven-dissipative dynamics in Ising-spin ensembles with power-law interactions. We point out the importance of fluctuations for the topology of the nonequilibrium phase diagram and draw a direct connection to the form of the spin-spin interactions. In particular, bistability cannot occur under the common assumption of pure van der Waals (vdW) interactions, but instead requires a short-distance dipolar potential core. Such a short-distance behavior is characteristic for Rydberg atoms [Fig. 1(b)], but typically neglected in theoretical models. Upon incorporating particle motion we reveal a temperature-driven phase transition to bistable nonequilibrium steady states. In the high-temperature limit we demonstrate a crossover to MF behavior, offering an explanation of thermal-vapor experiments [8].

We consider a random ensemble of N two-level systems with states $|g_i\rangle$ and $|e_i\rangle$ $(i = 1,\ldots,N)$ coupled by a laser field with a Rabi frequency Ω and frequency detuning Δ [Fig. 1(a)]. The associated unitary dynamics is governed by the Hamiltonian $\hat{H} = \frac{\Omega}{2}\sum_i (|e_i\rangle\langle g_i| + |g_i\rangle\langle e_i|) - \Delta\sum_i |e_i\rangle\langle e_i| + \sum_{i<j} V(r_{ij})|e_i e_j\rangle\langle e_i e_j|$, where $V(r_{ij})$ denotes the interaction potential of two particles at positions $\mathbf{r}_i$ and $\mathbf{r}_j$ and $r_{ij} = |\mathbf{r}_j - \mathbf{r}_i|$. The N-body density matrix, $\hat{\rho}$, of the system evolves according to the master equation $\dot{\hat{\rho}} = -i[\hat{H},\hat{\rho}] + \mathcal{L}[\hat{\rho}]$. The Lindblad superoperator $\mathcal{L}[\hat{\rho}] = \sum_{i,\alpha}(L_{i,\alpha}\hat{\rho}L_{i,\alpha}^\dagger - \frac{1}{2}L_{i,\alpha}^\dagger L_{i,\alpha}\hat{\rho} - \frac{1}{2}\hat{\rho}L_{i,\alpha}^\dagger L_{i,\alpha})$ describes one-body decoherence processes. We account for decay of the excited state ($L_{i,0} = \sqrt{\Gamma}|g_i\rangle\langle e_i|$) with a rate Γ and de-phasing of the laser-driven transition ($L_{i,1} = \sqrt{\gamma}|e_i\rangle\langle e_i|$) with a rate γ.

From now on we use dimensionless quantities, scaling time by Γ^{-1} and length by the critical radius r_b, defined as the particle distance at which $V(r_\mathrm{b}) = \Gamma + \gamma$. We consider a potential [23]

$$\frac{V(\bar{r})}{\Gamma+\gamma} = \frac{1-\sqrt{1+\xi^6/\bar{r}^6}}{1-\sqrt{1+\xi^6}}, \tag{1}$$

which features a dipolar potential core ($V \sim 1/r^3$) below a distance r_vdW and vdW interactions ($V \sim 1/r^6$) for $r > r_\mathrm{vdW}$. Here $\bar{r} = r/r_\mathrm{b}$, and $\xi = r_\mathrm{vdW}/r_\mathrm{b}$ denotes the vdW distance

*nikolasibalic@physics.org

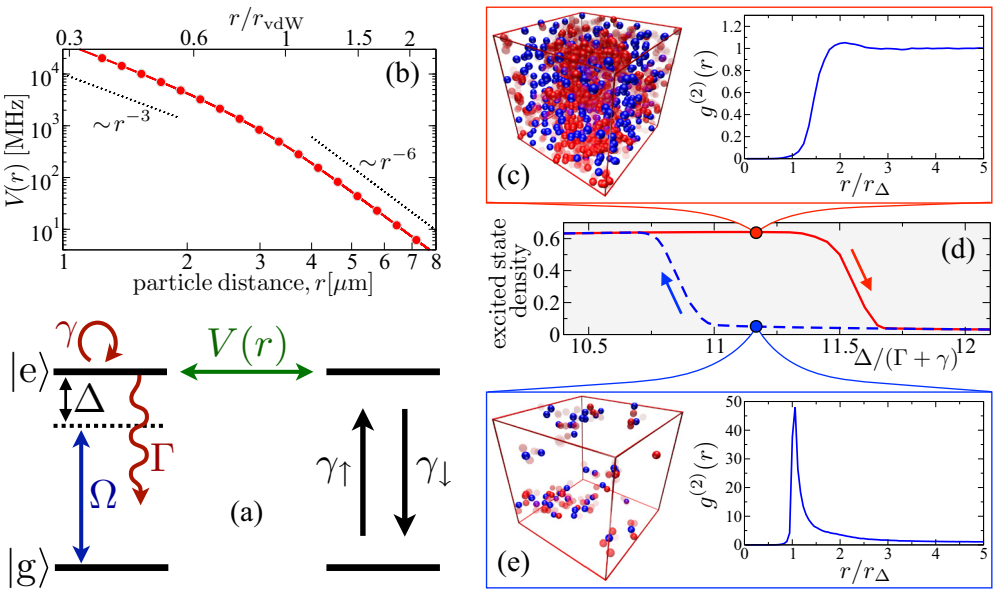

FIG. 1. (a) An ensemble of interacting two-level systems is driven coherently with a coupling strength Ω and frequency detuning Δ in the presence of decay and dephasing with rates Γ and γ, respectively. (b) The potential Eq. (1) (solid line) interpolates between different power laws and accurately describes the actual interaction between excited rubidium atoms (dots), shown for Rb($70S_{1/2}$) atoms. (d) Hysteresis with bistable steady states, whose typical spatial configurations and correlation functions are illustrated in panels (c) and (e). Blue spheres show excited particles, while the opacity of the red dots indicates the excitation rate $\gamma_\uparrow$ of particles in state $|g\rangle$.

relative to the blockade radius. Since r_b defines the typical distance between Rydberg atoms limited by the excitation blockade, the value of ξ characterizes the importance of dipolar interactions. Equation (1) reproduces the characteristics of Rydberg atom interactions [6], as illustrated in Fig. 1(b) by a comparison to numerical results [24] for $nS_{1/2}$ states of rubidium atoms.

Provided that $\Omega/(\Gamma+\gamma) \ll 1$ one can adiabatically eliminate the dynamics of the off-diagonal density-matrix elements and obtain a closed evolution equation for the diagonal $\rho_{\mathbf{S},\mathbf{S}}$ [25–28]. The matrix elements $\rho_{\mathbf{S},\mathbf{S}}$ describe the population of N-body configurations $\mathbf{S} \equiv (s_1,\ldots,s_N)$. Here, s_i is an effective spin variable denoting the ground ($s_i = 0$) and excited ($s_i = 1$) state of the ith particle. Introducing the state vector $\mathbf{S}_i \equiv (s_1,\ldots,1-s_i,\ldots,s_N)$, the resulting master equation can be written as

$$\dot{\rho}_{\mathbf{S},\mathbf{S}} = -\sum_i \left[s_i\gamma_\downarrow^{(i)}(\mathbf{S}) + (1-s_i)\gamma_\uparrow^{(i)}(\mathbf{S})\right]\rho_{\mathbf{S},\mathbf{S}} + \sum_i \left[s_i\gamma_\uparrow^{(i)}(\mathbf{S}) + (1-s_i)\gamma_\downarrow^{(i)}(\mathbf{S})\right]\rho_{\mathbf{S}_i,\mathbf{S}_i}, \quad (2)$$

where the single-body (de)excitation rates are given by $\gamma_\uparrow^{(i)} \equiv \bar{\Omega}^2/[1+4\bar{\Delta}_i(\mathbf{S})^2]$ and $\gamma_\downarrow^{(i)} \equiv 1+\gamma_\uparrow^{(i)}$. The rates are determined by two parameters: the scaled Rabi frequency $\bar{\Omega} = \Omega/\sqrt{\Gamma(\Gamma+\gamma)}$ and the scaled frequency detuning $\bar{\Delta}_i(\mathbf{S}) = \Delta_i(\mathbf{S})/(\Gamma+\gamma)$. The latter consists of the laser detuning Δ and the interaction-induced level shifts from nearby excited particles, $\Delta_i(\mathbf{S}) = \Delta - \sum_{j\neq i} V(r_{ij})s_j$ [27].

Exact quantum-trajectory simulations for small systems [29] established the accuracy of this approach for $\Omega \ll \Gamma+\gamma$. Note that this condition does not restrict our parameters and permits $\bar{\Omega} \gtrsim 1$ if $\gamma > \Gamma$, as will be assumed for throughout this article. This condition is often well fulfilled in experiments, with, e.g., $\gamma \sim 10^3\Gamma$ for conditions of the measurements on cold Rubidium gases reported in Ref. [7,30]. Here, one typically finds a large number of interaction potentials converging to different pair asymptotes [see Fig. 2(a)]. Yet, such additional potentials and associated molecular states are either not coupled or are only weakly coupled by the laser field [24,31,32], such that the excitation dynamics and steady states are expectedly well described by the single model potential Eq. (1), as illustrated in Fig. 2(b) for two interacting Rb($60S_{1/2}$) atoms.

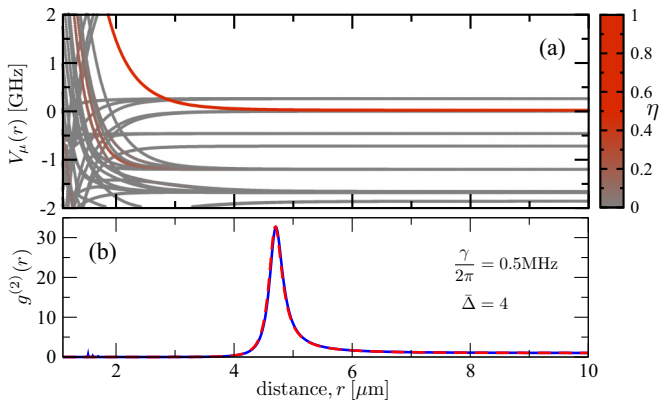

FIG. 2. (a) Potential curves $V_\mu(r)$ near the $(60S_{1/2},60S_{1/2})$ asymptote of rubidium atoms. The color code $\eta = \Omega_\mu^2/\Omega^2$ shows the Rabi coupling, Ω_μ, to a given molecular pair state $|\mu\rangle$ relative to that (Ω) of the noninteracting $(60S_{1/2},60S_{1/2})$ pair state [22]. (b) Steady-state Rydberg-Rydberg atom correlation function for $\bar{\Omega} = 1$ and the parameters indicated in the figure. Apart from very weak and narrow resonances at small distances the full multilevel calculations (solid blue line) agree well with the results obtained for the simplified model potential Eq. (1) (red dashed line).

In the case of large ensembles, the obtained effective master equation can be solved via kinetic Monte Carlo (MC) sampling [33]. To this end, we randomly sample N particle positions from a cubic volume with periodic boundary conditions and an edge length L, chosen to be much larger than r_b and r_{vdW}. The corresponding dimensionless density $\rho = Nr_b^3/L^3$ defines the number of particles within a given blockade volume r_b^3. To calculate the excitation spectrum, we perform positive and negative scans of the detuning $\bar{\Delta}$ with a corresponding chirp rate $\pm\kappa$. Observables are calculated from an ensemble average over many realizations of particle disorder configurations.

We find two distinct steady states with low and high excitation density ρ_e. The low-density phase corresponds to a dilute gas of excited pairs [Fig. 1(e)], formed by resonant sequential excitation of particles at a distance r_Δ for which the potential $V(r_\Delta) = \Delta$ compensates the detuning. The correlations in high-density phase [Fig. 1(c)] do not feature strong ordering on the length scale r_Δ and resemble a liquid of repulsive excitations.

To investigate the stability of these two phases, we calculate the excitation spectrum for negative and positive scans of the detuning. For a proper choice of parameters, both phases are indeed found to coexist over a finite range of $\bar{\Delta}$ where the excitation density shows hysteretic behavior, showing qualitative resemblance to MF predictions [11]. However, in contrast to MF expectations [14], we find no evidence of bistability for pure vdW interactions ($\xi \to 0$). This is illustrated in Figs. 3(a) and 3(b) where we show typical excitation spectra for small and large values of the vdW radius. For small ξ, the excitation blockade prevents particles from exploring the dipolar region of the interaction potential and one finds a smooth resonance curve with a unique steady state. However, once the short-distance $1/r^3$ behavior of $V(r)$ starts to become significant, the system develops bistable steady states beyond a critical driving strength [Fig. 3(b)].

This behavior can be understood by considering the effect of the potential form on energy level fluctuations. Spontaneous decay inevitably causes $|e\rangle \to |g\rangle$ transitions and thereby temporal fluctuations of the corresponding interaction-induced

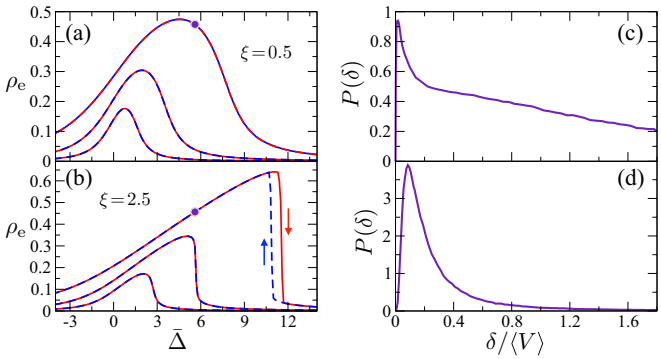

FIG. 3. (a, b) Excitation spectrum for $\rho = 10$ and $\bar{\Omega} = 1$, 0.5, and 0.25 (from top to bottom), obtained from positive (red solid line) and negative (blue dashed line) frequency scans as indicated by the arrows. (c, d) Distribution of potential fluctuations, δ, for parameters indicated by the dots in panels (a) and (b).

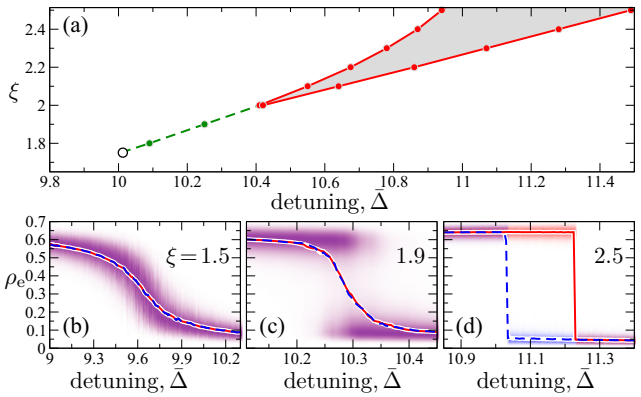

FIG. 4. Phase diagram for $\rho = 10$ and $\bar{\Omega} = 1$, showing a bistable region (gray area) and first-order phase transition (dashed green line) between low- and high-ρ_e phases, which ends in a critical point (open circle) at $1.7 < \xi < 1.8$. (b–d) Excitation density from a single stochastic trajectory. The blue solid and red dashed lines show the average excitation density for different scan directions, while the color shading indicates the corresponding probability distribution of ρ_e.

level shifts Δ_i. For $\xi \lesssim 1$, the total level shift, Δ_i, of an excited particle typically results from a small number of excitations in close proximity. Hence, a single decay event will cause a substantial change of Δ_i and disturb the excitation dynamics. The resulting large density fluctuations [Fig. 4(b)] prevent the formation of two distinct phases. For large ξ, a large number of excitations within a distance $\lesssim \xi$ collectively contribute to Δ_i, such that potential fluctuations are greatly reduced. To validate this picture, we have traced the microscopic steady-state dynamics for two different values of ξ and otherwise identical parameters and average densities, ρ_e [dots in Fig. 3(a) and 3(b)]. By recording the maximum change, δ, of the level shift of excited particles due to a de-excitation, we construct the spectrum of potential fluctuations $P(\delta)$ from the long-time microscopic steady state dynamics. As seen in Fig. 3(c), one indeed finds a broad distribution for $\xi = 0.5$ with extended tails well beyond the average potential shift $\langle V\rangle$. On the contrary, for $\xi = 2.5$ [Fig. 3(d)] $P(\delta)$ is sharply peaked around small $\delta \ll \langle V\rangle$ and drops rapidly for larger values. It is this strong suppression of fluctuations [Fig. 4(d)] that facilitates the formation of bistable steady states in the limit of large ξ.

The microscopic steady-state dynamics provides further insights about the transition between these two regimes. The nonequilibrium phase diagram shown in Fig. 4(a) reveals a finite region of bistability at large ξ which ultimately closes upon decreasing ξ. In between these two limits, the low- and high-density phases, coexisting as long-lived metastable states, are connected by a first-order phase transition over a finite range of ξ. This transition, generally obscured by the ensemble average over random particle configurations, is revealed by the counting statistics of a single N-body trajectory, as demonstrated in Figs. 4(b)–4(d) where we show the excitation-density distribution for a single particle configuration at a low chirp rate $\kappa = 10^{-8}$. For $1.8 \lesssim \xi \lesssim 2$ both phases dynamically coexist and yield a *persistent* bimodal counting statistics. The ensemble average of the corresponding

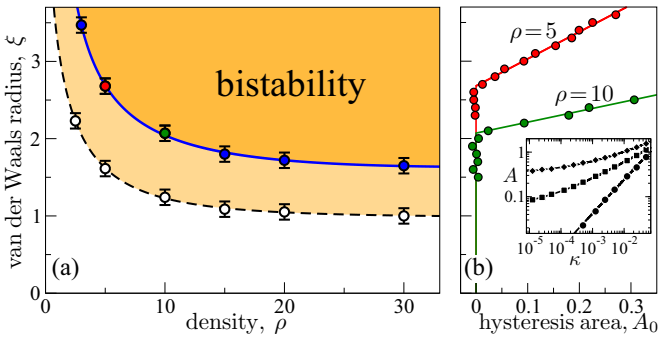

FIG. 5. (a) $\xi - \rho$ phase diagram for $\bar{\Omega} = 1$, obtained from MC simulations of frozen particles (solid circles) and eaMF calculations (open circles). Panel (b) shows the static hysteresis area, A_0, from the frozen-gas simulations for two different densities. The inset illustrates the typical dependence of A on the chirp rate κ for $\rho = 10$ and $\xi = 1.7$ (circles), 2.1 (squares), and 2.5 (diamonds). The lines show a fit to $A = A_0 + a\kappa^{-b}$, with free parameters A_0, a, and b.

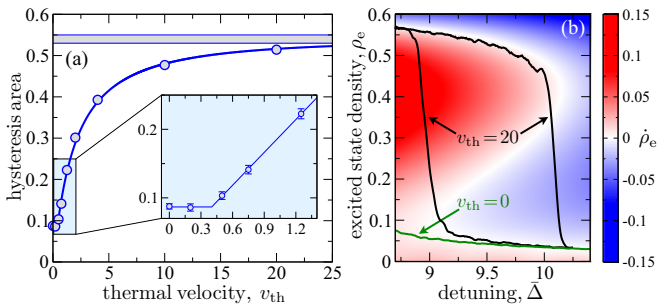

FIG. 6. (a) Hysteresis area as a function of thermal velocity for $\bar{\Omega} = 0.8$, $\xi = 2$, $\rho = 10$, $L = 12$, and $\kappa = 2.2 \times 10^{-3}$. The data indicate a continuous phase transition around $v_{\rm th} \approx 0.4$ and approach the eaMF prediction shown by the gray horizontal bar. Statistical errors correspond to the symbol size and the height of the bar. The color code in panel (b) shows $\dot{\rho}_{\rm e}$ from the eaMF approach. The numerical high-temperature simulations ($v_{\rm th} = 20$) closely follow the bistable eaMF steady state ($\dot{\rho}_{\rm e} = 0$) in contrast to the monostable behavior at $v_{\rm th} = 0$.

transition point yields the first-order transition line shown in Fig. 4(a), which ends in a critical point around $1.7 < \xi < 1.8$.

For a broader characterization of the conditions leading to bistability we have calculated the asymptotic hysteresis area A_0 by extrapolating $A(\kappa)$ to the limit $\kappa \to 0$ [inset of Fig. 5(b)]. Upon changing ξ, A_0 indicates a continuous transition with a critical exponent ~ 1 [Fig. 5(b)]. The critical ξ expectedly decreases with particle density [Fig. 5(a)]. Yet, the apparent saturation of the transition line at large densities provides further indication for the absence of bistable behavior for systems with dominant vdW interactions ($\xi < 1$).

In order to verify the occurrence of a transition we have further studied the average switching time between the two steady states and indeed found the a power-law divergence upon approaching the critical detunings shown in Fig. 4(a). Yet, the corresponding exponents vary with ξ, which stands in contrast to thermal-vapor experiments [8] that observed a universal MF exponent of 0.5 [34]. To resolve this issue we now consider thermal particle motion which diminishes correlations and thereby alters the spectrum of fluctuations. For simplicity we neglect interparticle forces and adopt an ideal gas description with an equilibrium velocity distribution and dimensionless thermal velocity $v_{\rm th}$, measured in units of $r_{\rm b}\Gamma$. Tracking the evolving particle positions now requires fixed-time-step MC simulations [33] of the spin dynamics.

As shown in Fig. 6(a), thermal motion drives a continuous phase transition to bistability. At high temperatures the hysteresis area saturates to a finite value that can be understood within the following MF treatment. Assuming that rapid thermal motion completely randomizes any spatial excitation structures, we can neglect correlations in Eq. (2) to obtain a closed equation, $\dot{\rho}_{\rm e} = \bar{\gamma}_\uparrow - (1 + 2\bar{\gamma}_\uparrow)\rho_{\rm e}$, for the average excitation density. Averaging the microscopic rates $\gamma_\uparrow^{(i)}$ over the uncorrelated ensemble yields a closed expression for the MF excitation rate

$$\bar{\gamma}_\uparrow = \frac{\bar{\Omega}}{2}\int_0^{+\infty} dk\, e^{-k\{1/2+\mathrm{Re}[f(k)]\}}\cos\left(k\{\Delta + \mathrm{Im}[f(k)]\}\right), \tag{3}$$

where $f(k) = k^{-1}\rho_{\rm e}\int 1 - e^{ikV(r)}d\mathbf{r}$ can be interpreted as the interaction-induced line shift [Im(f)] and broadening [Re(f)]. As shown in Figs. 6(a) and 6(b), our high-temperature results indeed approach this ensemble averaged mean-field (eaMF) limit. In contrast to corresponding lattice MF models [14,17,18], the functional $\rho_{\rm e}$ dependence of $\bar{\gamma}_\uparrow$ depends strongly on the shape of the interaction potential. In particular, for $\xi = 0$ one finds $\mathrm{Re}(f) = \mathrm{Im}(f) \propto \rho_{\rm e}\sqrt{k}$, which implies that no phase transition can occur for pure vdW interactions. The numerically obtained eaMF transition line (Fig. 5) demonstrates that this remains true for finite $\xi < 1$.

Finally, we put our findings into the context of recent experiments. Reference [7] reports bimodal counting statistics of Rydberg excitations in a cold gas of Rb atoms excited to $70S_{1/2}$ states. The quoted laser linewidth $\gamma/2\pi \approx 500$ kHz and Rabi frequencies $\Omega < (\Gamma + \gamma)$ are within the regime of validity of the present theory. However, the scaled vdW radius of $\xi \approx 0.3$ implies that the conditions of Ref. [7] do not promote bistable steady states according to the results presented in this work. We are thus lead to conclude that bimodal Rydberg atom distribution observed in Ref. [7] does not indicate the emergence of bistability [14] or a phase transition [17,18] in the steady state of the system. We point out, however, that bimodality at finite excitation times, τ, can result from transient relaxation effects [29,35], while for larger τ dipolar state mixing induced by black-body radiation [36,37] on a time scale $\tau_{\rm bbr} < \tau$ [7,38] significantly affects the gas dynamics as observed in other recent experiments [32,39–41]. Note that the temperature corresponding to a thermal velocity of $r_{\rm b}\Gamma$, for typical values of $r_b \approx 11\,\mu$m and $\Gamma^{-1} \approx 200\,\mu$s [7], can be as low as $\sim 30\,\mu$K such that atom motion can be a factor even in cold-gas experiments. Consequently, thermal gases [8,42] are deep in the high-temperature limit, $v_{\rm th} \gg 1$, and their measured excitation dynamics can therefore be understood within the outlined eaMF approach, which thus appears more appropriate than the frozen gas assumption [42]. Importantly, the thermally activated transition to MF behavior explains the emergence of the dynamical MF exponents [14,34] observed in Ref. [8]. Beyond the physics of interacting Rydberg atoms, the results

of our work are of direct relevance to the nonequilibrium behavior of other systems such as cold polar molecules [43] or laser-cooled ion crystals [5,44] that permit realization of synthetic spin systems with tunable driving and dissipation as well as controllable power-law interactions with variable exponents [44].

In summary, we have investigated driven dissipative spin ensembles with competing power-law interactions. The steady state of our master equation (2) shares the same MF limit as that [9,14] obtained from the exact quantum evolution, yet it accounts for classical correlations and fluctuations which we showed to be important for the nonequilibrium physics of such systems. As a striking consequence, the specific shape of the interaction potential was found to play a key role for the nonequilibrium phase diagram despite its general finite-range nature, dropping rapidly as $\sim 1/r^6$. This motivates further studies on the suggested universality of such systems both in theory and experiments. Experimentally, the spatial extent of the inner dipolar potential can be tuned by external static [45] or microwave [46] fields, which should permit explorations of the predicted phase diagram (Figs. 4 and 5) in future measurements. We showed that thermal particle motion can drive a transition to bistablity and ultimately causes MF behavior to emerge. The nonequilibrium phase transition takes place at a surprisingly low temperatures in the μK to mK domain, which should enable its observation in cold atom experiments. The established high-temperature MF limit (eaMF) permitted an analytical proof for the importance of the inner potential core and provides a consistent explanation of recent thermal-vapor experiments [8]. The simplicity of the derived approach should moreover enable future extensions to multilevel excitation schemes and more complex interactions that may occur in such systems [8,42].

We thank Rick van Bijnen, Simon Gardiner, Hendrik Weimer, and Igor Lesanovsky for valuable discussions. This work was supported by the EU through the FET-Open Xtrack Project HAIRS, the FET- PROACT Project RySQ, and the Marie-Curie ITN COHERENCE and also by Durham University and the UK EPSRC Grants No. EP/M014398/1 and No. EP/M013103/1.

The data presented in this paper are available [47].

[1] J. W. Gibbs, *Elementary Principles in Statistical Mechanics* (Cambridge University Press, Cambridge, UK, 1902).
[2] L. M. Sieberer, M. Buchhold, and S. Diehl, arXiv:1512.00637 [Rep. Prog. Phys. (to be published)].
[3] H. Ritsch, P. Domokos, F. Brennecke, and T. Esslinger, Rev. Mod. Phys. **85**, 553 (2013).
[4] I. Carusotto and C. Ciuti, Rev. Mod. Phys. **85**, 299 (2013).
[5] J. W. Britton, B. C. Sawyer, A. C. Keith, C.-C. J. Wang, J. K. Freericks, H. Uys, M. J. Biercuk, and J. J. Bollinger, Nature (London) **484**, 489 (2012).
[6] M. Saffman, T. Walker, and K. Mølmer, Rev. Mod. Phys. **82**, 2313 (2010).
[7] N. Malossi, M. M. Valado, S. Scotto, P. Huillery, P. Pillet, D. Ciampini, E. Arimondo, and O. Morsch, Phys. Rev. Lett. **113**, 023006 (2014).
[8] C. Carr, R. Ritter, C. G. Wade, C. S. Adams, and K. J. Weatherill, Phys. Rev. Lett. **111**, 113901 (2013).
[9] T. E. Lee, H. Häffner, and M. C. Cross, Phys. Rev. A **84**, 031402(R) (2011).
[10] T. E. Lee, S. Gopalakrishnan, and M. D. Lukin, Phys. Rev. Lett. **110**, 257204 (2013).
[11] T. E. Lee, H. Häffner, and M. C. Cross, Phys. Rev. Lett. **108**, 023602 (2012).
[12] A. Hu, T. E. Lee, and C. W. Clark, Phys. Rev. A **88**, 053627 (2013).
[13] M. Höning, D. Muth, D. Petrosyan, and M. Fleischhauer, Phys. Rev. A **87**, 023401 (2013).
[14] M. Marcuzzi, E. Levi, S. Diehl, J. P. Garrahan, and I. Lesanovsky, Phys. Rev. Lett. **113**, 210401 (2014).
[15] C. Ates, B. Olmos, J. P. Garrahan, and I. Lesanovsky, Phys. Rev. A **85**, 043620 (2012).
[16] I. Lesanovsky and J. P. Garrahan, Phys. Rev. A **90**, 011603(R) (2014).
[17] H. Weimer, Phys. Rev. Lett. **114**, 040402 (2015).
[18] H. Weimer, Phys. Rev. A **91**, 063401 (2015).
[19] M. F. Maghrebi and A. V. Gorshkov, Phys. Rev. B **93**, 014307 (2016).
[20] M. Hoening, W. Abdussalam, M. Fleischhauer, and T. Pohl, Phys. Rev. A **90**, 021603(R) (2014).
[21] J. J. Mendoza-Arenas, S. R. Clark, S. Felicetti, G. Romero, E. Solano, D. G. Angelakis, and D. Jaksch, Phys. Rev. A **93**, 023821 (2016).
[22] C. Gaul, B. J. DeSalvo, J. A. Aman, F. B. Dunning, T. C. Killian, and T. Pohl, Phys. Rev. Lett. **116**, 243001 (2016).
[23] W. Li, P. J. Tanner, and T. F. Gallagher, Phys. Rev. Lett. **94**, 173001 (2005).
[24] R. M. W. van Bijnen and T. Pohl, Phys. Rev. Lett. **114**, 243002 (2015).
[25] A. Chotia, M. Viteau, T. Vogt, D. Comparat, and P. Pillet, New J. Phys. **10**, 045031 (2008).
[26] C. Ates, T. Pohl, T. Pattard, and J. M. Rost, J. Phys. B At. Mol. Opt. Phys. **39**, L233 (2006).
[27] C. Ates, T. Pohl, T. Pattard, and J. M. Rost, Phys. Rev. A **76**, 013413 (2007).
[28] C. Ates, T. Pohl, T. Pattard, and J. M. Rost, Phys. Rev. Lett. **98**, 023002 (2007).
[29] D. W. Schonleber, M. Garttner, and J. Evers, Phys. Rev. A **89**, 033421 (2014).
[30] M. M. Valado, C. Simonelli, M. D. Hoogerland, I. Lesanovsky, J. P. Garrahan, E. Arimondo, D. Ciampini, and O. Morsch, Phys. Rev. A **93**, 040701(R) (2016).
[31] Y.-Y. Jau, A. M. Hankin, T. Keating, I. H. Deutsch, and G. W. Biedermann, Nat. Phys. **12**, 71 (2015).
[32] J. Zeiher, R. V. Bijnen, P. Schauß, S. Hild, J.-Y. Choi, T. Pohl, I. Bloch, and C. Gross, arXiv:1602.06313 (unpublished).
[33] K. A. Fichthorn and W. H. Weinberg, J. Chem. Phys. **95**, 1090 (1991).
[34] G. Grynberg and S. Cribier, J. Phys. Lett. **44**, 449 (1983).

[35] H. Schempp, G. Günter, M. Robert-de-Saint-Vincent, C. S. Hofmann, D. Breyel, A. Komnik, D. W. Schönleber, M. Gärttner, J. Evers, S. Whitlock, and M. Weidemüller, Phys. Rev. Lett. **112**, 013002 (2014).
[36] T. F. Gallagher and W. E. Cooke, Phys. Rev. Lett. **42**, 835 (1979).
[37] W. E. Cooke and T. F. Gallagher, Phys. Rev. A **21**, 588 (1980).
[38] I. I. Beterov, I. I. Ryabtsev, D. B. Tretyakov, and V. M. Entin, Phys. Rev. A **79**, 052504 (2009).
[39] T. Amthor, M. Reetz-Lamour, S. Westermann, J. Denskat, and M. Weidemüller, Phys. Rev. Lett. **98**, 023004 (2007).
[40] E. A. Goldschmidt, T. Boulier, R. C. Brown, S. B. Koller, J. T. Young, A. V. Gorshkov, S. L. Rolston, and J. V. Porto, Phys. Rev. Lett. **116**, 113001 (2016).
[41] B. J. DeSalvo, J. A. Aman, C. Gaul, T. Pohl, S. Yoshida, J. Burgdörfer, K. R. A. Hazzard, F. B. Dunning, and T. C. Killian, Phys. Rev. A **93**, 022709 (2016).
[42] A. Urvoy, F. Ripka, I. Lesanovsky, D. Booth, J. P. Shaffer, T. Pfau, and R. Löw, Phys. Rev. Lett. **114**, 203002 (2015).
[43] S. A. Moses, J. P. Covey, M. T. Miecnikowski, B. Yan, B. Gadway, J. Ye, and D. S. Jin, Science **350**, 659 (2015).
[44] J. G. Bohnet, B. C. Sawyer, J. W. Britton, M. L. Wall, A. M. Rey, M. Foss-feig, and J. J. Bollinger, Science **352**, 1297 (2016).
[45] T. Vogt, M. Viteau, A. Chotia, J. Zhao, D. Comparat, and P. Pillet, Phys. Rev. Lett. **99**, 073002 (2007).
[46] S. Sevinçli and T. Pohl, New J. Phys. **16**, 123036 (2014).
[47] N. Šibalić, C. G. Wade, C. S. Adams, K. J. Weatherill, and T. Pohl, *Data for "Driven-Dissipative Many-Body Systems with Mixed Power-Law Interactions: Bistabilities and Temperature-Driven Nonequilibrium Phase Transitions"*, http://dx.doi.org/10.15128/r1w08929926.